J|A|C|S ARTICLES

Published on Web 03/10/2009

Bottom-up Design of Hybrid Polymer Nanoassemblies Elucidates Plasmon-Enhanced Second Harmonic Generation from Nonlinear Optical Dyes

Miki Ishifuji, Masaya Mitsuishi,* and Tokuji Miyashita

Institute of Multidisciplinary Research for Advanced Materials (IMRAM), Tohoku University, 2-1-1 Katahira, Aoba-ku, Sendai 980-8577, Japan

Received November 7, 2008; Revised Manuscript Received February 6, 2009; E-mail: masaya@tagen.tohoku.ac.jp

Abstract: Flexible design of hybrid polymer nanoassemblies consisting of nonlinear optical (NLO) polymer nanosheets and gold nanoparticle alignment was done to elucidate near-field effects of localized surface plasmon (LSP) coupling, which was generated from coupled gold nanoparticles, on enhanced second harmonic generation (SHG) from nonlinear optical (NLO) dyes in hybrid nanoassemblies. Structurally well-defined hybrid polymer nanoassemblies comprising NLO polymer nanosheets and aligned gold nanoparticles were fabricated using bottom-up approaches: Langmuir−Blodgett (LB) technique and nanoparticle adsorption. Two hybrid polymer nanoassembled structures were particularly examined: a single-layer NLO polymer nanosheet and gold nanoparticle monolayer (single-layer structure) exhibiting intralayer LSP coupling, and a single-layer NLO polymer nanosheet sandwiched between two-layer gold nanoparticle monolayers (sandwich structure). The latter enables interlayer LSP coupling between the two gold nanoparticle monolayers. Dependence of SHG intensity on the distance between the NLO layer and nanoparticle layer was examined according to the LB layer structure and gold nanoparticle size variation. The SH light intensity from the NLO polymer nanosheet decreased almost exponentially with increasing spacer distance between the NLO polymer nanosheet and gold nanoparticle monolayer in both single-layer and sandwich structures. The decay length depends strongly on the gold nanoparticle size, indicating effective spatial distance for enhanced SHG from NLO polymer nanosheets. Theoretical calculations were used to study the enhancement mechanism. Finite difference time domain (FDTD) calculations reproduced the exponential behavior of SH light intensity as a function of separation distance, which confirmed the importance of coupled gold nanoparticle formation and parallel geometry of near-field coupling of the coupled gold nanoparticles with NLO polymer nanosheets for efficient SHG enhancement. Dipole-type LSP coupling along the long axis of adjacent gold nanoparticles at the fundamental frequency dominates enhancement of SHG from NLO dyes oriented parallel to the long axis of LSP coupling, which occurs at the center of the Au NPs.

Introduction

Many nanosized materials have remarkable properties. Noble metal nanoparticles such as gold nanoparticles (Au NPs) and silver nanoparticles (Ag NPs), for example, have unique optical properties and localized surface plasmon resonance (LSPR).[1−7] The single-metal nanoparticles can induce collective oscillation of conductive electrons, localized surface plasmons, at the metal surface when irradiated with visible light. When the localized surface plasmon is excited, a strongly enhanced electromagnetic field is formed at the particle surface, which provides new plasmon-based applications for chemicals and biosensors.[8] Recently, metal nanoparticle assemblies have been studied because stronger electromagnetic field enhancement occurs at nanoparticle junctions than occurs with isolated nanoparticles.[9] The LSPR from each single-metal nanoparticle can be coupled electromagnetically when they are near each other. The enhancement of the electromagnetic field induced by coupled LSPR is a few orders of magnitude greater than that by a single-metal nanoparticle. To date, localized surface plasmons from metal nanostructures created mainly using top-down approaches have been investigated intensively to elucidate the enhancement of emissive processes and nonlinearities.[10−16] However, very

(1) Kreibig, U., Vollmer, M. *Optical Properties of Metal Clusters*; Springer: Berlin, 1995.
(2) Hutter, E.; Fendler, J. H. *Adv. Mater.* **2004**, *16*, 1685–1706.
(3) Ghosh, S. K.; Pal, T. *Chem. Rev.* **2007**, *107*, 4797–4862.
(4) Willets, K. A.; Van Duyne, R. P. *Annu. Rev. Phys. Chem.* **2007**, *58*, 267–297.
(5) Maier, S. A. *Plasmonics: Fundamentals and Applications*; Springer: New York, 2007.
(6) Pelton, M.; Aizpurua, J.; Bryant, G. *Laser Photonics Rev.* **2008**, *2*, 136–159.
(7) Watanabe, K.; Menzel, D.; Nilius, N.; Freund, H. J. *Chem. Rev.* **2006**, *106*, 4301–4320.
(8) Lee, J. S.; Ulmann, P. A.; Han, M. S.; Mirkin, C. A. *Nano Lett.* **2008**, *8*, 529–533.
(9) Hao, E.; Schatz, G. C. *J. Chem. Phys.* **2004**, *120*, 357–366.
(10) Lippitz, M.; van Dijk, M. A.; Orrit, M. *Nano Lett.* **2005**, *5*, 799–802.
(11) Nappa, J.; Russier-Antoine, I.; Benichou, E.; Jonin, C.; Brevet, P. F. *J. Chem. Phys.* **2006**, *125*, 184712.
(12) Russier-Antoine, I.; Benichou, E.; Bachelier, G.; Jonin, C.; Brevet, P. F. *J. Phys. Chem. C* **2007**, *111*, 9044–9048.
(13) Bouhelier, A.; Bachelot, R.; Lerondel, G.; Kostcheev, S.; Royer, P.; Wiederrecht, G. P. *Phys. Rev. Lett.* **2005**, *95*, 267405.

10.1021/ja808749h CCC: $40.75

small features such as particle separation of less than 10 nm are difficult to fabricate lithographically.[17]

Hybrid nanomaterials made of organic and inorganic nanomaterials are expected to produce noble and innovative functions that might not be achieved from either component alone. Moreover, nanoscale hybrid nanoassemblies present the great potential to support development of small, inexpensive, and highly efficient devices. Construction of hybrid nanoassemblies requires well-ordered and uniform accumulation of hybrid nanomaterials at the nanointerface. Different bottom-up approaches are useful for construction of hybrid nanoassemblies. Some examples are the layer-by-layer (LbL)[18] method, self-assembled monolayers (SAMs),[19] and Langmuir−Blodgett (LB) technique.[20] The advantages of such bottom-up approaches depend upon the fact that design features are related to the hybrid nanoassemblies' unique physical characteristics based on supramolecular chemistry. We demonstrated the advantages of polymer LB films, as exemplified by an amphiphilic polymer poly(*N*-dodecylacrylamide) (pDDA).[21] We can introduce various functional molecules into the polymers properly and uniformly, providing a functional polymer LB film.[22−25] Recently, we defined stable polymer LB films as "polymer nanosheets". We reported that the hybrid polymer nanoassemblies of nonlinear optical (NLO) polymer nanosheets with Au NPs provide enormous second harmonic (SH) light enhancement derived from a coupled LSPR.[26]

Regarding plasmon-enhanced second harmonic generation (SHG), increasingly numerous reports have described experimental and theoretical considerations.[27−34] Most reports have specifically addressed SHG from the metal nanostructure itself, with several carrying hybrid nanoassemblies with metal nanostructure and NLO dyes. The lack of spatial effects of LSPR on SHG has also been investigated because of the difficulty in precise positioning of metal nanoparticles[35] as well as the difficulty of controlling the NLO dye orientation in hybrid nanoassemblies at the nanometer scale. Because SHG from dye molecules correlates with molecular nonlinear polarization,[36] detailed investigations of SHG from NLO dyes enhanced by LSPR offers a new fundamental scientific insight related with light−matter interaction based on LSPR. Herein, we describe the flexible design of hybrid polymer nanoassemblies, aiming at deep understanding of plasmon-enhanced SHG in terms of the structure−property relation. We quantitatively investigated coupled LSPR using NLO polymer nanosheets. The salient advantage of the LB technique is the attractive design of hybrid nanoassemblies in both two-dimensional (2D) and 3D fields.[37] Using polymer nanosheets, we can control the interparticle spacing of Au NPs carefully at nanometer-length scale.[38] The localized surface plasmon (LSP) coupling is *near-field* coupling localized at the particle surface. Therefore, it is of great importance to position Au NPs and NLO polymer nanosheets with nanoscale precision for elucidation of structure−property relations associated with SHG enhancement of coupled LSPR.

Numerous studies have examined the distance-dependence of LSPR by SERS,[39] luminescence,[38] and UV−vis extinction[40−42] spectra. We used SHG for probing the nanoscale electromagnetic fields of coupled LSPR. The SH light intensity shows a quadratic response to the electric field magnitude. Therefore, we can obtain specific information related to changes in LSPR. Two methods were examined for respective results on SH light enhancement, as presented in Scheme 1. Using the first method, effects of coupled LSPR and NLO polymer nanosheets were assessed by varying the separation distance between NLO polymer nanosheets and Au NPs (fixed interparticle distance) (single-layer structure) as well as the size of Au NPs. The second method varied the interparticle distance between Au NPs in which NLO polymer nanosheets were located at the center of two-layer Au NPs (sandwich structure). Experimental results were compared with finite difference time domain (FDTD) calculations[43] in terms of structure−property relation between NLO polymer nanosheets and intralayer and interlayer LSP coupling.

Experimental Section

Hybrid Polymer Nanoassembly with Gold Nanoparticles. Two-layer cationic p(DDA/VPy) nanosheets were deposited on hydrophobic glass substrates at the surface pressure and temperature of 35 mN/m and 15 °C; then they were immersed in Au NP aqueous

(14) Ueno, K.; Juodkazis, S.; Mizeikis, V.; Sasaki, K.; Misawa, H. *Adv. Mater.* **2008**, *20*, 26–30.
(15) Bozhevolnyi, S. I.; Beermann, J.; Coello, V. *Phys. Rev. Lett.* **2003**, *90*, 197403.
(16) Sung, J.; Hicks, E. M.; Van Duyne, R. P.; Spears, K. G. *J. Phys. Chem. C* **2007**, *111*, 10368–10376.
(17) Canfield, B. K.; Husu, H.; Laukkanen, J.; Bai, B. F.; Kuittinen, M.; Turunen, J.; Kauranen, M. *Nano Lett.* **2007**, *7*, 1251–1255.
(18) Decher, G.; Schlenoff, J. B. *Multilayer Thin Films: Sequential Assembly of Nanocomposite Materials*; Wiley-VCH: New York, 2002.
(19) Ulman, A. *An Introduction to Ultrathin Organic Films from Langmuir-Blodgett to Self-Assembly*; Academic Press: San Diego, CA, 1991.
(20) Petty, M. C. *Langmuir-Blodgett Films*; Cambridge University Press: Cambridge, U.K., 1996.
(21) Mitsuishi, M.; Matsui, J.; Miyashita, T. *J. Mater. Chem.* **2009**, *19*, 325–329.
(22) Kim, Y.; Zhao, F.; Mitsuishi, M.; Watanabe, A.; Miyashita, T. *J. Am. Chem. Soc.* **2008**, *130*, 11848–11849.
(23) Kado, Y.; Mitsuishi, M.; Miyashita, T. *Adv. Mater.* **2005**, *17*, 1857–1861.
(24) Parvin, S.; Sato, E.; Matsui, J.; Miyashita, T. *Polym. J.* **2006**, *38*, 1283–1287.
(25) Mitsuishi, M.; Matsui, J.; Miyashita, T. *Polym. J.* **2006**, *38*, 877–896.
(26) Ishifuji, M.; Mitsuishi, M.; Miyashita, T. *Appl. Phys. Lett.* **2006**, *89*, 011903.
(27) Sandrock, M. L.; Pibel, C. D.; Geiger, F. M.; Foss, C. A. *J. Phys. Chem. B* **1999**, *103*, 2668–2673.
(28) Moran, A. M.; Sung, J. H.; Hicks, E. M.; Van Duyne, R. P.; Spears, K. G. *J. Phys. Chem. B* **2005**, *109*, 4501–4506.
(29) Hayakawa, T.; Usui, Y.; Bharathi, S.; Nogami, M. *Adv. Mater.* **2004**, *16*, 1408–1412.
(30) McMahon, M. D.; Lopez, R.; Haglund, R. F.; Ray, E. A.; Bunton, P. H. *Phys. Rev. B* **2006**, *73*, 041401.
(31) Hubert, C.; Billot, L.; Adam, P. M.; Bachelot, R.; Royer, P.; Grand, J.; Gindre, D.; Dorkenoo, K. D.; Fort, A. *Appl. Phys. Lett.* **2007**, *90*, 181105.
(32) Simon, M.; Trager, F.; Assion, A.; Lang, B.; Voll, S.; Gerber, G. *Chem. Phys. Lett.* **1998**, *296*, 579–584.
(33) Chen, K.; Durak, C.; Heflin, J. R.; Robinson, H. D. *Nano Lett.* **2007**, *7*, 254–258.
(34) Vallius, T.; Jefimovs, K.; Turunen, J.; Vahimaa, P.; Svirko, Y. *Appl. Phys. Lett.* **2003**, *83*, 234–236.
(35) Sandrock, M. L.; Foss, C. A. *J. Phys. Chem. B* **1999**, *103*, 11398–11406.
(36) Shen, Y. R. *Principles of Nonlinear Optics*; John Wiley: New York, 1984.
(37) Ishifuji, M.; Mitsuishi, M.; Miyashita, T. *Chem. Commun.* **2008**, 1058–1060.
(38) Tanaka, H.; Mitsuishi, M.; Miyashita, T. *Chem. Lett.* **2005**, *34*, 1246–1247.
(39) Ringler, M.; Klar, T. A.; Schwemer, A.; Susha, A. S.; Stehr, J.; Raschke, G.; Funk, S.; Borowski, M.; Nichtl, A.; Kurzinger, K.; Phillips, R. T.; Feldmann, J. *Nano Lett.* **2007**, *7*, 2753–2757.
(40) Haynes, C. L.; McFarland, A. D.; Zhao, L. L.; Van Duyne, R. P.; Schatz, G. C.; Gunnarsson, L.; Prikulis, J.; Kasemo, B.; Kall, M. *J. Phys. Chem. B* **2003**, *107*, 7337–7342.
(41) Huang, W. Y.; Qian, W.; Jain, P. K.; El-Sayed, M. A. *Nano Lett.* **2007**, *7*, 3227–3234.
(42) Reinhard, B. M.; Siu, M.; Agarwal, H.; Alivisatos, A. P.; Liphardt, J. *Nano Lett.* **2005**, *5*, 2246–2252.
(43) Taflove, A. *Computational Electromagnetics: The Finite-Difference Time-Domain Method*; Artech House: Boston, MA, 2005.

Scheme 1. Schematic Illustration of Hybrid Polymer Nanoassembly Fabrication.

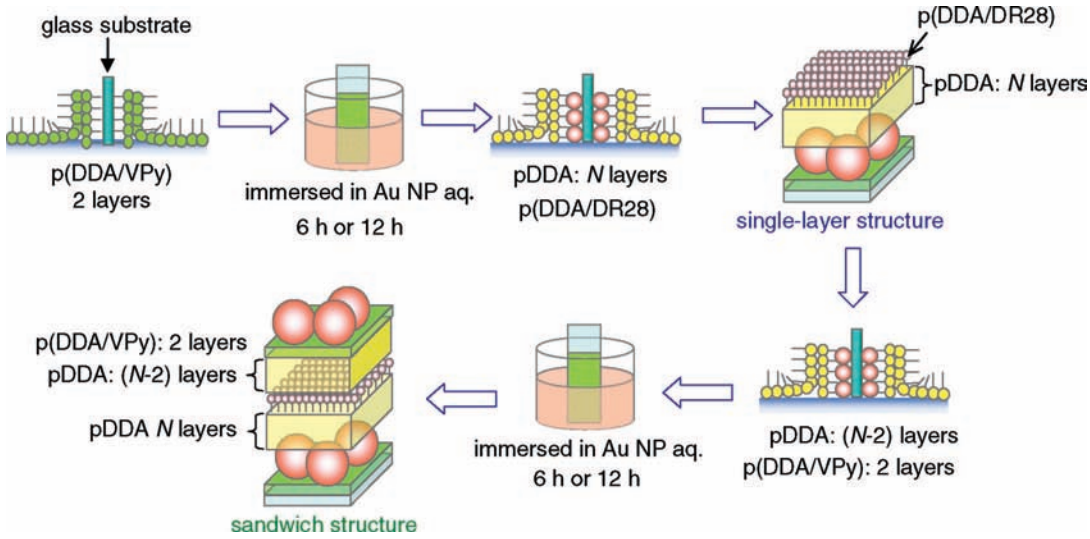

solution in a refrigerator for respective times. After immersion, the substrate was washed with distilled water and dried using nitrogen gas. In these processes, Au NPs were immobilized uniformly on p(DDA/VPy) nanosheets through electrostatic interaction. *N*-layer (N = 2, 6, 10, and 18 for 30-nm-diameter Au NPs, N = 2, 4, 6, and 10 for 12-nm-diameter Au NPs) pDDA spacer nanosheets were deposited on Au NP monolayers, and then a single-layer p(DDA/DR28) nanosheet was deposited (single-layer structure) (Scheme 1). For the sandwich structure, (*N*-2)-layer pDDA spacer nanosheets were deposited on the single-layer structure. Then, two-layer p(DDA/VPy) nanosheets were deposited, followed by immersion in Au NP aqueous solution for 6 or 12 h. A single-layer p(DDA/DR28) nanosheet was located in the center of the sandwich structure. The pDDA nanosheet was used for controlling the separation distance between Au NPs and the p(DDA/DR28) nanosheet.

Measurements. Optical SHG measurements were carried out using the Maker fringe method.[44] Details of the optical setup are described in Supporting Information. The SH light intensity of the sample at an incident angle of 45° was determined by normalizing the Maker fringe envelope with that from a Y-cut quartz. The film thickness of the sandwich structure was characterized using a surface profiler (Dektak ^{3}ST; Ulvac Technologies Inc.). All measurements were carried out at room temperature.

FDTD Calculations. Finite difference time domain (FDTD) calculations were carried out using a commercially available program (FDTD solutions 6.0; Lumerical Solutions, Inc.).[6,7] For those calculations, we used a workstation (64 GB RAM, Precision T7400; Dell Computer Corp.) with good processing capabilities (3.0 GHz Xeon X5450; Intel Corp.). The simulation region was set to be 150 × 150 × 150 nm^3 with perfectly matched layer conditions imposed at the boundaries. The gold nanoparticle diameter was set to 30 nm. Typical simulations were ranged around 300 fs. We located Au NPs at designated positions surrounded by vacuum. Total-field scattered-field sources, which separate the simulation area into two regions, total-field (incident plus scattered field)- and scattered-field-only regions, were used to calculate the scattering and absorption cross sections. For this study, the incident field is defined as a plane wave with a wave vector that is normal to the injection surface. The scattered and total fields were monitored during the simulation such that the total or scattered transmission was measurable.[8] A mesh override region was set to 1 nm around the Au NPs to minimize simulation times and maximize the resolution of field enhancement regions around Au NP sphere. The dispersion-dependent function of Au NP was described by the modified Drude model with plasma frequency $\omega_p = 1.38 \times 10^{16}$ s^{-1} and collision frequency $\upsilon_c = 1.075 \times 10^{14}$ s^{-1}. (see Supporting Information). Using different geometries of Au NPs, 3D calculations were performed. Spatial electric field distribution at 1064 nm as well as the electric field enhancement at the center of the cell were obtained.

Results and Discussion

SHG from Hybrid Polymer Nanoassemblies: Single-Layer Structure. NLO polymer nanosheets consisting of poly(*N*-dodecylacrylamide) (pDDA) and poly[*N*-dodecylacrylamide-co-4′-([2-acryloyloxyethyl]ethylamino)-4-nitroazobenzene]s (p(DDA/DR)s) (Figure 1) exhibit good SHG properties at the monolayer level (Figure S4, Supporting Information). The SH light intensity from hybrid polymer nanoassemblies with 12-h immersion time was enhanced by a factor of 8 over that of NLO polymer nanosheets without Au NPs (Figure S6, Supporting Information). No SH light enhancement occurred with less than 8-h immersion time.[26] The average interparticle distance was estimated from SEM images as more than 100 nm at 6-h immersion time; consequently, no interaction occurred between these Au NPs. As the immersion time increased, the number of Au NPs immobilized on the polymer nanosheets increased, thereby engendering a red-shift and broadening of the LSPR band (Figure S7b, Supporting Information). The ESEM image of the sample with 12-h immersion time in Figure S8b, Supporting Information showed the appearance of two adjacent Au NPs along with isolated Au NPs. In other words, intralayer LSP coupling occurred between two adjacent Au NPs, thereby creating a red-shift of the extinction band. Further immersion in Au NP aqueous solution (20 h) provided two distinct extinction bands (Figure S7c,

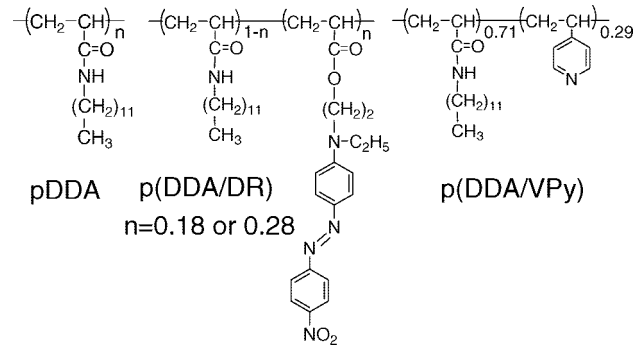

Figure 1. Chemical structures of amphiphilic polymers used for this study.

(44) Chen, C. K.; Heinz, T. F.; Ricard, D.; Shen, Y. R. *Phys. Rev. B* **1983**, *27*, 1965–1979.

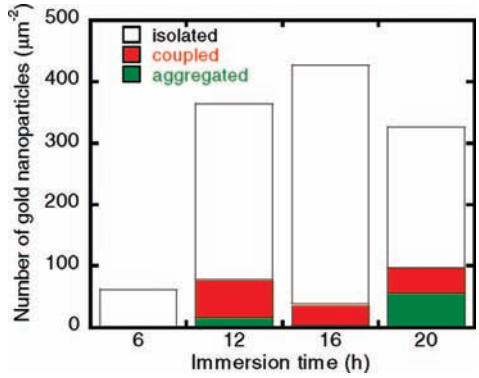

Figure 2. Number of Au NPs adsorbed onto p(DDA/VPy) nanosheets in the hybrid polymer nanoassemblies as a function of immersion time.

Supporting Information), reflecting aggregate formation with more than two Au NPs (Figure S8c, Supporting Information). The peak position of the "aggregates" (678 nm) differed from that of coupled Au NPs, although both bands broadened to 1500 nm.

To obtain further detailed information related to Au NP adsorption, we examined the number of Au NPs with various ensemble situations: isolated, coupled, and aggregated states (Figure 2). As described above, the aggregated state corresponded to the Au NP ensembles consisting of more than two gold nanoparticles. For 12-h immersion time (the optimized immersion time for SHG enhancement in the single-layer structure[26]) 79% Au NPs existed as isolated, 16% as form-coupled, and 5% as form-aggregated. The ratio of the coupled Au NPs was the largest in all single-layer structures with different immersion times. For 16 and 20 h, the ratio of coupled Au NPs decreased, and the SH light intensities became less than those measured after 12 h of immersion.[26] We therefore inferred that coupled Au NPs, not aggregates, are most effective for strong electric field enhancement of SHG. The coupled Au NPs enhanced the electromagnetic field at the fundamental light (1064 nm),[44] thereby enhancing the SH light at 532 nm from DR.

Effects of Separation Distance between p(DDA/DR) Nanosheets and Au NP Monolayer and Au NP Size on SH Light Intensity. Intralayer LSP coupling occurs at the nanometer-length scale around the metal nanoparticle surface because the LSPR is optical near-field excitation. Therefore, the electric field that is enhanced by the LSP coupling is attenuated concomitantly with increasing distance from the metal surface. Because the pDDA nanosheet has a monolayer thickness of 1.7 nm, the pDDA nanosheet serves as a good nanoruler to control the distance between the NLO polymer nanosheet and the Au NP monolayer at the nanometer scale. We inserted spacer pDDA nanosheets ($N = 2$, 6, 10, and 18 layers) between the single-layer p(DDA/DR28) nanosheet and a Au NP monolayer (single-layer structure). Numerous reports in the relevant literature describe effects of the distance between Au NPs on LSP coupling using extinction spectroscopy.[39,41,42,45,46] In this case, the distance between coupled Au NPs and the single-layer p(DDA/DR28) nanosheet was adjusted two-dimensionally in the single-layer structure. In other words, we can probe the electric field distribution of coupled LSPRs in line with the substrate surface normal. Figure 3 depicts the SH light intensity from the single-layer structure (incident angle = 45° with respect to the surface normal) as a function of the distance T (in nm) between the single-layer p(DDA/DR28) nanosheet and the Au NP monolayer. The SH light intensity in Figure 3 decreased exponentially. From fitting with a single exponential function, we determined the decay length $d_{1/e}$, of which the SH light

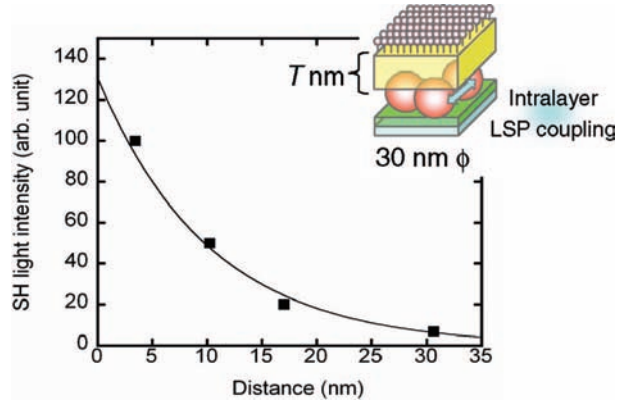

Figure 3. SH light intensity from a single-layer structure as a function of the separation distance between Au NPs (30 nm ϕ) and a p(DDA/DR28) nanosheet (inset).

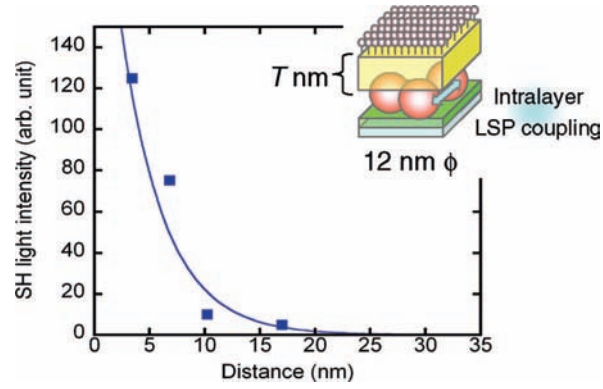

Figure 4. SH light intensity from a single-layer structure as a function of the separation distance between Au NPs (12 nm ϕ) and a p(DDA/DR28) nanosheet (inset).

intensity fell to 1/e: 8.4 nm. This value indicates that effective LSP coupling for SH light enhancement occurred within a distance of 8.4 nm from the Au NP monolayer.

In addition, SHG enhancement was observed using a smaller Au NP (12 nm ϕ). The decay length depends strongly on the Au NP size (Figure 4). The $d_{1/e}$ value for a 12-nm-diameter Au NP was determined to be 4.0 nm. The Au NP size dependence on the $d_{1/e}$ value is convincing evidence that the SH light intensity reflects coupled LSPR. Quantitative analysis offered excellent prospects of positioning functional molecules in hybrid polymer nanoassemblies for LSPR-based optoelectronic devices.

SHG from Hybrid Polymer Nanoassemblies: Sandwich Structure. The SH light intensity from a sandwich structure (12-h immersion time) achieved 36-fold enhancement compared to that from using single-layer Au NPs (Figure S9, Supporting Information). This enhancement corresponds to 288-fold enhancement compared to that of a pristine single-layer NLO polymer nanosheet. The SH light enhancement results from interlayer LSP coupling between two adjacent Au NPs assembled perpendicular to the substrate in addition to intralayer LSP coupling. It must be added that no remarkable SHG signal was obtained from the sandwich structure without a p(DDA/DR) nanosheet. In other words, the SHG contribution from Au NPs is negligible: we observed plasmon-enhanced SHG only from the p(DDA/DR) nanosheet in our

(45) Jain, P. K.; Huang, W. Y.; El-Sayed, M. A. *Nano Lett.* **2007**, *7*, 2080–2088.
(46) Su, K. H.; Wei, Q. H.; Zhang, X.; Mock, J. J.; Smith, D. R.; Schultz, S. *Nano Lett.* **2003**, *3*, 1087–1090.

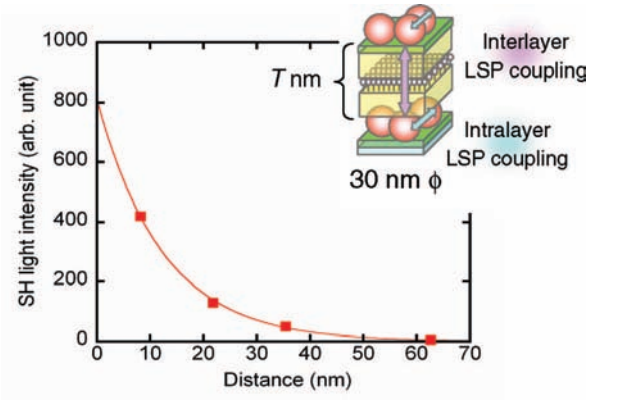

Figure 5. SH light intensity from the sandwich structure (12-h immersion time) as a function of the separation distance between two Au NP monolayers.

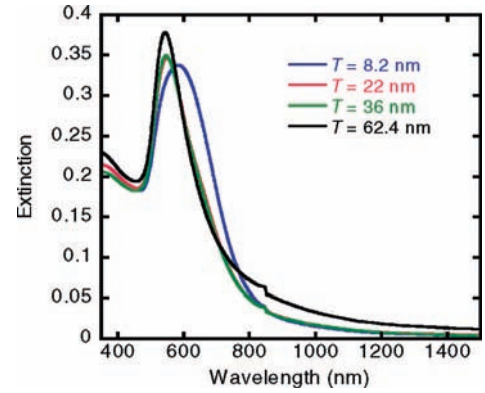

Figure 6. Extinction spectra of sandwich structures (12-h immersion time) with different separation distances between Au NP monolayers.

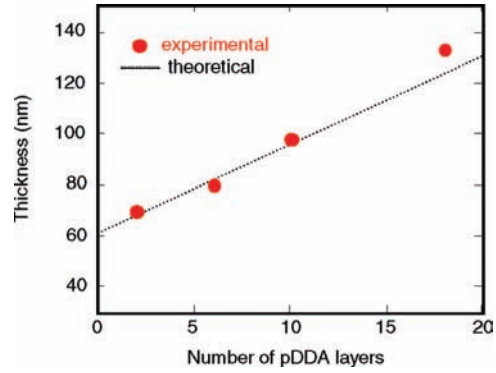

Figure 7. Sandwich structure (6-h immersion time) thickness as a function of the number of pDDA spacer layers.

experimental conditions. Considering the polymer nanosheet thickness, the separation distance between Au NPs in interlayer LSP coupling can be estimated as less than 10 nm. The number density of the coupled Au NPs was estimated using scanning electron microscopy and atomic force microscopy as 60 (μm^{-2}) and 30 (μm^{-2}), respectively, for intralayer and interlayer LSP coupling. Two inferences can be drawn from these results. First, strong electric field enhancement occurs by coupled LSPR. For that reason, the interparticle spacing in interlayer LSP coupling is less than that in intralayer LSP coupling. Second, the dipole-like electromagnetic interaction of the LSPR with nonlinear polarization is much more effective in interlayer LSP coupling because LSP coupling has a dipole-like character. In the next section, we examine the structure−property relation of LSP coupling for SH light enhancement.

Effect of Separation Distance between Interlayer Au NP Monolayers on SH Light Intensity. We inserted pDDA spacer (N = 2, 6, 10, and 18 layers) into the sandwich structure to elucidate the distance dependence on LSP coupling with the interlayer Au NP monolayer in the sandwich structure (Scheme 1). The immersion time in Au NP aqueous solution was 12 h for both first and second Au NP adsorption, indicating that both intralayer and interlayer LSP coupling contribute to the SH light enhancement. Each Au NP maintained equal distance from a centrally located p(DDA/DR28) nanosheet. Figure 5 depicts the SH light intensity from the sandwich structure as a function of separation distance. Similar to the single-layer structure, the SH light intensity decreased exponentially with increasing separation distance. Previously, Su et al. reported that the coupled LSPR showed that plasmon shift decayed exponentially as the intralayer Au NP distance increased.[46] Recently, Lal et al. reported the exponential decay of surface-enhanced Raman scattering (SERS) intensity with increasing distance from the Au nanoshell.[47] These exponential behaviors are explainable as dipolar-type LSP coupling.[1,45] Therefore, the distance dependence of SH light intensity in the single-layer and sandwich structure is dominated by dipole LSP coupling. The UV−vis−NIR extinction spectra in Figure 6 represent the extent of the interaction between intralayer and interlayer LSP coupling. The nearest distance between Au NPs (N = 2) showed a red-shift and broadening in the LSPR band, indicating that the strongest LSPR interaction occurred. The LSPR band moved toward a shorter wavelength because of the increased distance between two-layer Au NPs. Finally, at the 18-layer (~30.6 nm) pDDA spacer, the LSPR band shape came to resemble that of single-layer Au NPs, meaning that Au NPs in each layer behave independently. The SH light enhancement in the sandwich structure with 18-layer pDDA spacer showed the same magnitude of SH light intensity as that of NLO polymer nanosheet without Au NPs. The $d_{1/e}$ value of the sandwich structure was determined as 12.8 nm. Similarly, the $d_{1/e}$ value for Au NPs (12 nm ϕ) was determined as 7.1 nm (see Figure S13, Supporting Information). These values involve the contribution of the intralayer and the interlayer LSP coupling at the 12-h (30 nm ϕ) or 4-h (12 nm ϕ) immersion time.

Regarding the contribution of intralayer and interlayer LSP coupling to SHG enhancement, we reported previously that it was possible to create only interlayer LSP coupling in the sandwich structure when the immersion time was set at less than 8 h for first and second Au NP adsorption.[37] We prepared another sandwich structure at 6-h immersion times for both first and second Au NP adsorption. We measured the film thickness (Figure S11, Supporting Information); Figure 7 portrays a comparison of experimental thickness measured using a surface profiler with theoretical thickness based on simple addition of respective thicknesses of pDDA, p(DDA/DR), and p(DDA/VPy) nanosheets and the diameter of Au NP. Experimental thickness results are similar to those of the theoretical thickness, indicating that we can control the distance between two-layer Au NPs precisely using a polymer nanosheet. Figure 8 portrays the SH light intensity from the sandwich structure as a function of the distance between interlayer Au NPs with an immersion time of 6 h. Exponential decay behavior was also observed between SH light intensity and

(47) Lal, S.; Grady, N. K.; Goodrich, G. P.; Halas, N. J. *Nano Lett.* **2006**, *6*, 2338–2343.

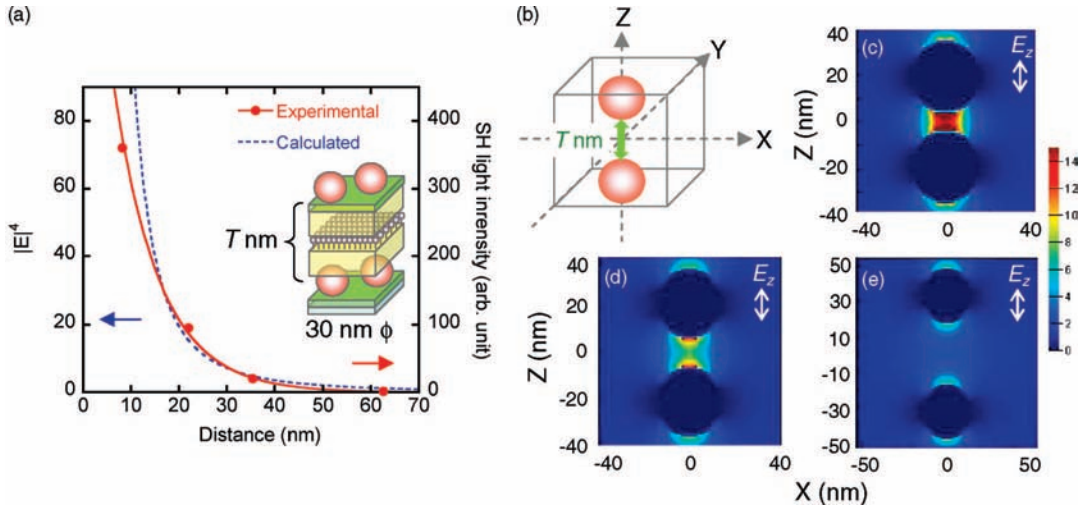

Figure 8. (a) Calculated electric field enhancement as a function of the separation distance between the interlayer Au NP (6-h immersion time) fitted curve with a single exponential calculated curve (solid), with FDTD calculation (dotted), and with experimental data (closed circles). (b) Schematic illustration of the geometry of Au NPs and the direction of irradiated light. (c−e) Electric field distribution between interlayer Au NPs as a function of separation distance with *Z*-polarized incident light.

interlayer Au NPs distance. The $d_{1/e}$ value was determined as 9.4 nm, smaller than that of 12-h immersion. This value is contributed solely by interlayer LSP coupling between two-layer Au NP monolayers. The $d_{1/e}$ for the intralayer or interlayer LSP coupling was estimated to be of a comparative order of magnitude. Detailed analyses of DR orientation on Au NPs and layer structure will further elucidate the effect of DR on near-field coupling with coupled LSPR. That work is now in progress.

Electric Field Enhancement of LSPR Calculated using the FDTD Method. Regarding LSP coupling between two Au NPs, strong electromagnetic field enhancement is observed when the polarization of the incident light is parallel to the interparticle long axis.[17] Electric field enhancement by LSP coupling is affected strongly by the distance separating Au NPs. The electric field generated by two Au NPs can be estimated using FDTD calculations.[48−50] We compared our experimental results of SH light enhancement at 6-h immersion time to the numerically calculated electric field distribution using FDTD (Figure 8). We simulated the electric field enhanced at 1064 nm by interlayer LSP coupling. Electric field enhancement for light polarization parallel to the dimer axis is portrayed in Figure 8. The intensity enhancement is directly related to the square of the electric field. The electric field enhancement and intensity at $(x, y, z) = (0, 0, 0)$ and $T = 8.2$ nm, the shortest distance in the experimental conditions, were calculated respectively as 3.77 and 14.26. Theoretically, the SH light intensity is proportional to the square of the fundamental laser light intensity: $|E|^4$.[36] Figure 8a portrays the electric field enhancement at 1064 nm calculated at $(x, y, z) = (0, 0, 0)$ as a function of the separation distance between two Au NPs. The calculated values show good agreement with that of the sandwich structure (9.4 nm for 6-h immersion time) without the exception of the value at $T = 8.2$ nm. In other words, the strong electric field enhancement parallel to the interparticle long axis coupled with incident light polarization at the fundamental frequency dominates the SHG enhancement from DR components. It must be explained that the calculated point at $T = 8.2$ nm is deviated from the fitted exponential function, which implies that dipole-like near-field coupling becomes more predominant at a spacer distance of less than 10 nm.

Electric field enhancement, as revealed by FDTD calculation, also enables estimation of the number of SH active molecules and estimation of the DR capability of interacting with LSP coupling for SH light enhancement. The effective cross-sectional area for LSP coupling was assumed to be 1.1×10^2 nm^2 (in the $X-Y$ plane), where the magnitude of the enhancement reached more than 80% of the maximum (red region in Figure 8c) and the number of DR molecules in the area was estimated to be 1.0×10^2. The number density of coupled Au NPs is determined to be 30 (μm^{-2}). Therefore, 0.33% of the DR in p(DDA/DR) nanosheet monolayer can undergo light-matter interaction with LSP coupling.

Finally, we carried out FDTD calculation to respond to the following question: why are coupled Au NPs, not aggregates, most effective for SHG enhancement? Experimentally, the SH light intensity decreased with greater than 12-h immersion (single-layer structure) at which time aggregate formation (not chain type) consisting of three more Au NPs was generated. In an earlier study, we observed suppression of the SH light intensity in a multilayer structure with 12-h immersion time.[37] In other words, aggregates with more than two Au NPs suppress the SH light intensity in both intralayer and interlayer LSP coupling. We simulated the electric field distribution of Au NP ensembles (Figure 9). Figure 9a depicts the geometry of the Au NP ensembles. The centers of the three Au NPs are located in the $X-Z$ plane. Two of them form LSP coupling with separation distance of 8.2 nm along the *Z* axis. One other Au NP is located on the *X* axis separately from the two Au NPs. The *Z*-polarized plane wave was used as incident light. We calculated the electric field distribution, moving the Au NP along the *X* axis while maintaining the two other Au NPs on the *Z* axis. The bottom part of Figure 9 presents the simulation results: the squared magnitude of the E_z component, which is parallel to the incident light polarization (Figure 9b,c), and those of perpendicular E_x component (Figure 9d,e). Lower near-field coupling occurred among the three Au NPs when the Au NP is far from the coupled Au NPs (the end-to-end distance is $T =$

(48) Futamata, M.; Maruyama, Y.; Ishikawa, M. *J. Phys. Chem. B* **2003**, *107*, 7607–7617.
(49) Zhang, J.; Fu, Y.; Chowdhury, M. H.; Lakowicz, J. R. *Nano Lett.* **2007**, *7*, 2101–2107.
(50) Brandl, D. W.; Mirin, N. A.; Nordlander, P. *J. Phys. Chem. B* **2006**, *110*, 12302–12310.

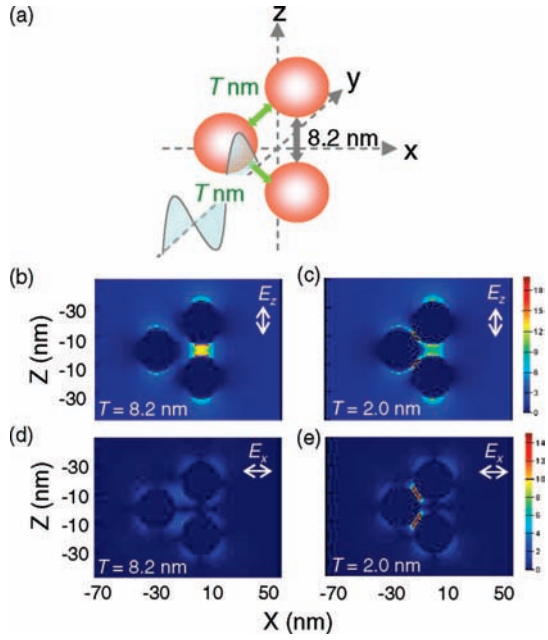

Figure 9. (a) Schematic illustration of the geometry of Au NPs and the direction of irradiated light. (bottom) FDTD calculation for electric field distribution using *Z*-polarized incident light with different coupled Au NP geometries: (b) *Z*-component electric field distribution at $T = 8.2$ nm; (c) *Z*-component electric field distribution at $T = 2.0$ nm; (d) *X*-component electric field distribution at $T = 8.2$ nm; (e) *X*-component electric field distribution at $T = 2.0$ nm.

8.2 nm, Figure 9b,d). The coupled Au NPs have a dipole-like LSP coupling character. However, the purely *Z*-polarized incident field induces a local E_x component at $T = 2.0$ nm, as depicted in Figure 9e, leading to the decreased E_z component (Figure 9c). The LSP coupling is distributed evenly between the left Au NP and right Au NP pair, changing its polarization direction. This LSP coupling "delocalization" and distribution suppress SHG enhancement because a parallel orientation of LSP coupling with DR polarization is necessary for obtaining strong SH light intensity. It is noteworthy that strong electric field enhancement of the E_x component also occurred between three Au NPs. This is very preferable for SHG enhancement because nonlinear optical phenomena are based on tensor mode polarization.[36,51] In fact, the SH light intensity from the sandwich structure with 12-h immersion time exhibited enormous SHG enhancement even when s-polarized light was used as the incident light (Figure 10). The FDTD method is useful for elucidating LSP coupling and for elucidating the enhancement of nonlinearity in terms of the structure−property relation.

Conclusions

We fabricated hybrid polymer nanoassemblies consisting of NLO polymer nanosheets and gold nanoparticles (Au NPs). We then characterized the structure−property relation of SH light enhancement by controlling the distance separating NLO polymer nanosheets and Au NPs at a nanometer-length scale. We assembled Au NPs and NLO polymer nanosheets at the nanometer-length scale and produced hybrid polymer nanoassemblies of two types using LB technique and immersion method: a single-layer structure and a sandwich structure.

(51) Prasad, P. N.; Williams, D. J. *Introduction to Nonlinear Optical Effects in Molecules and Polymers*; Wiley-Interscience: New York, 1991.

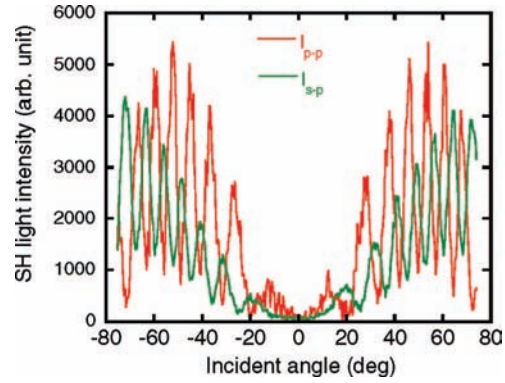

Figure 10. SH fringe patterns from a sandwich structure (12-h immersion time) obtained using p-polarized light (red) and s-polarized light (green).

Intralayer and interlayer localized surface plasmon (LSP) coupling from adjacent Au NPs enhanced the SH light intensity efficiently. We investigated the distance-dependence on SH light intensity by inserting a pDDA spacer between NLO polymer nanosheets and Au NPs (single-layer structure) or between two-layer Au NPs (sandwich structure). The exponential decay of SH light intensity as a function of distance demonstrates that dipole-like LSP coupling at the fundamental frequency dominates SHG enhancement from hybrid polymer nanoassemblies. The quantitative results of $d_{1/e}$ demonstrate that we can control the LSP coupling in hybrid polymer nanoassemblies on a nanometer scale using the LB technique. We demonstrate the structure−property relation in terms of enhanced SHG, comparing experimental data with results obtained from FDTD calculations. Interestingly, the results suggest that the electric field enhancement at fundamental frequency alone is insufficient to achieve SHG enhancement: the resonance frequency and the polarization direction of enhanced electric field by LSP coupling with regard to the nonlinear optical component are also important for SHG enhancement. That is an appropriate explanation of why we were unable to elicit enhanced SHG from aggregates with more than two Au NPs. These findings will provide tremendous possibilities of hybrid polymer nanoassemblies for opening up new scientific fields related to nano-optics and nanophotonics based on bottom-up approaches.

Acknowledgment. We thank the Hybrid Nano-Materials Research Center (HyNaM Center), Tohoku University for the use of AFM and ESEM. This work was supported by Grants-in-Aid for Scientific Research (S) (No. 17105006) from the Japanese Society for the Promotion of Science (JSPS) and for Priority Area (No. 470) from the Ministry of Education, Culture, Sports, Science and Technology of Japan. M.I. also thanks the JSPS for a Research Fellowship.

Supporting Information Available: Experimental details of synthesis and preparation of NLO polymer nanosheet, measurements, and FDTD calculations. UV−vis absorption spectra of multilayered heterotype NLO polymer nanosheets. Characterization of NLO properties of heterotype polymer nanosheets using optical waveguide spectroscopy. ESEM images of hybrid polymer nanoassemblies. SHG properties of hybrid polymer nanoassemblies with 12-nm-diameter Au NPs. This material is available free of charge via the Internet at http://pubs.acs.org.

JA808749H